Advances in Science and Technology Research Journal

Advances in Science and Technology Research Journal, 2026, 20(2), 153–170
https://doi.org/10.12913/22998624/211667
ISSN 2299-8624, License CC-BY 4.0

Received: 2025.08.28
Accepted: 2025.11.15
Published: 2025.12.23

Experimental investigation of fracture orientation effects on bone dynamics behavior through vibration analysis

Jignesh Jani[1], Nikunj Rachchh[1*]

[1] Department of Mechanical Engineering, Marwadi University, Rajkot, 360003, Gujarat, India
* Corresponding author's e-mail: nikunj.rachchh@marwadieducation.edu.in

ABSTRACT

Conventional diagnostic tools for identifying fractures in bone, like X-rays and CT scans, are widely used, but involve ionizing radiation and lack sensitivity to physical degradation, like stiffness loss and damping in bones. To overcoe these limitations, non-invasive vibration-based diagnostic techniques are emerging as promising alternatives for evaluating fracture severity. This work aimed to assess the dynamic behavior of bone specimens with varying fracture orientations specifically oblique, longitudinal, and lateral to identify which orientation leads to the most severe mechanical degradation. Goat metacarpal bones were tested with four fracture types with an unfractured reference bone. Controlled lateral impacts were applied using an instrumented hammer, and vibrational responses were recorded using an accelerometer. Data were analyzed using Fast Fourier Transform (FFT) to extract Frequency Response Functions (FRF), coherence, and phase characteristics. Each condition was subjected to three tests for consistencies in results. The results indicated that lateral fractures resulted in the greatest decrease in stiffness, lowest resonance frequency, and largest FRF magnitude, making them the worst fracture type in mechanical degradation. This method has implications for radiation-free fracture diagnosis, particularly of benefit to pregnant women and radiation-sensitive groups.

Keywords: bone fracture diagnosis, vibration analysis, frequency response function, non-invasive diagnostic testing, fracture orientation.

INTRODUCTION

Bone fracture diagnosis is a critical aspect of orthopedic practice. Technological improvements lead to an upgraded quality of life for the living and improved mobility of instruments. Frequent use of instruments like X-rays, CT scans, and MRIs emits radiation into living things and damages tissue, but when it comes to results, radiation-based methods prove to be the gold standard benchmark across the globe in orthopedic diagnosis [1, 2] Researchers and scientists tried to develop alternative methods to discover musculoskeletal complications, which help in orthopedic medicine. Lippmann was the first researcher to apply auscultatory percussion across fractures of femur shaft, humerus, and clavicle bone to diagnose musculoskeletal disease using vibration-based non-invasive methods, in which interpreted as indicating the presence of a complete fracture [3]. The concept of assessment of musculoskeletal diseases by applying vibration-based techniques originated since the early twentieth century. Notable attention to low-frequency vibration analysis in orthopaedics began emerging in the early 1970s. With advancements in signal analysis technologies, late 1980s to early 1990s focused on the effort to develop vibration-based techniques into reliable clinical diagnostic tools. A notable example of this progress ejected by European study led by Professor G. Van der Perre with collaborators, explored the application of vibration analysis in orthopaedic assessments [4]. In 1996, Lowet and Vander Perre [5] measured the velocity of transverse waves on the tibia and reported an average speed of about of wave travel 1050 m/s. However, this value is low compared to newer studies. For example, Bossy

et al. [6] in 2002 reported a velocity of 2900 m/s. A possible reason for the discrepancy in Lowet and Vander Perre's results could be the interference from the waves caused by reflections at the bone ends. In 1987, Chen and Saha [7] developed a theoretical model of stress wave propagation by strike one end of the bone with a steel ball and monitoring the wave using strain gauges. They observed the stress pulses broadened as they travelled along the bone. However, their experiments were conducted in vitro, so their findings may not fully consider in vivo conditions due to the confirmed presence of muscle and soft tissues.

In 2021, Sim at el. [8] conducted in vivo testing by firing a pellet onto a metal disc positioned at the proximal end of a long bone and recording the resulting response using an accelerometer. To address the issue of skin interference, commonly regarded as a potential source of error in experimental studies, Vander Perre and Lower [4] introduced an impulse technique in which an excitation needle and recording accelerometer were placed directly onto the bone following a local injection of 1% xylocaine. Safaei et al. [9] developed an experimental approach to study degenerative joint conditions. Preliminary findings indicated predominant vibration frequencies in the range of 150 to 250 Hz; however, no pathological cases were documented in the study. In 2022, Do HD et al. [10] evaluated the mechanical properties of tibia in vivo condition using external impact techniques, which involve an impact hammer and an accelerometer. The impact measures the force and the peak amplitudes of the decaying vibration response; the mechanical impedance was determined. It is of interest to note that they suggested the measurement should be made by one experimenter in order to minimize variation in transducer preload.

In 2012, Razaghi et al. [11] conducted in vivo experiments by applying impact on the tibia of human volunteers using an impact hammer. The input force and the corresponding response displayed on a dual-beam oscilloscope, with the accelerometer signal channel triggered by the hammer to facilitate comparison of time differences between the signals. In the same year,

Recent studies have applied impulse excitation on fractured bones and compared vibrational responses across fracture sites to evaluate healing. Yoon et al. [12] demonstrated that the ratio of proximal to distal transverse vibration signals can be used to distinguish fracture conditions, while Sim et al. [8] further investigated the influence of boundary conditions on fracture vibration response.

Further in vivo investigations into impact response measurements of long bones were carried out. In the study by Chittibabu et al. [13] a conventional medical reflex hammer was used to gently strike the medial malleolus of the lower leg, with four samples recorded per subject. Additional patient-specific data, including height, weight, age, sex, and tibial length, were also collected to support the analysis.

Pattijin et al. [14] combined methods to investigate the modal analysis of the human lower leg. The excitation inputs include the impulse signals generated by hammer impacts on the tibia, although the specific impact location was not reported. In a notable study by Nokes [15] in 1999, various signal types were explored to stimulate bone response signals. These included impact signals, slow swept sine waves, and spectral excitation responses. The study did not identify a single optimal excitation method; instead, the authors concluded that the choice of signal may depend on the differing objectives of clinicians and engineers, noting that these requirements could potentially be in conflict due to varied research perspectives. In 2022, Scanlan et al. [16] applied an input impulse of approximately 0.5 ms to excite the tibia within a frequency range of up to 450 Hz. The data was used to develop a simplified beam model representing the vibratory behavior of the tibia.

Guo et al. [17] introduced a novel measurement device involving a calibrated weighted plunger to deliver impulsive forces to tibia in vivo condition. A similar approach was again reported by Mattei et al. [18] in the context of assessing fracture healing by measuring transverse vibrations in long bones. In this study, the impulse force applied directly to fixation nails of an external 'Orthofix' device, which had been temporarily removed during the procedure. The limb stabilized using a vacuum beanbag while the excitation was applied through nails screwed into the tibia, allowing direct transmission of the stimulus. In 2018, Verdenelli et al. [19] examined the use of elastic wave propagation to evaluate the mechanical properties of the human tibia. Their experimental setup involved an impact hammer with four strain gauges, with the following vibrations captured by two accelerometers placed distally along the bone. Fracture orientation plays an important role to identify the severity of a broken bone, which serves as a high mechanical impact

on bone [20–22]. Consider common clinical fracture types (longitudinal, transverse, and oblique). In this study, four fracture orientations were experimentally simulated: lateral (perpendicular to bone axis), longitudinal (parallel to axis), and 45° oblique (left-to-right and right-to-left). Each orientation of fracture affects stiffness and vibrational parameters differently [23–26].

In 2021, Gautam and Rao [27] introduced a non-contact measurement approach using a position sensing detector to assess the mechanical properties of the femur bone. Through natural frequency measurements and modal analysis, the method enabled nondestructive evaluation and determined the elastic modulus of the bone to be 14.8 GPa. Yoon et al. [12] introduces modal assurance criterion that employed to differentiate between healthy and fractured bones based on their vibration responses.

Although X-rays, CT scans, and MRIs are commonly used to detect bone fractures, they mainly show images of the bone structure but do not provide detailed information about how the bone strength and stiffness are affected after a fracture. Also, some limitations to these procedures are that they expose to radiation, can be costly, and are not always accessible, particularly in remote or less-equipped locations. More importantly, these radiation methods often cannot measure the severity of a fracture in terms of how much the bone's ability to resist force has changed. This creates a gap in current orthopedic diagnostic medical tools. To bridge this gap, vibration-based non-invasive methods offer a safe and low-cost way to assess bone health. By using a small, controlled strike and observing how the bone vibrates in response, the method can be used to detect variations in stiffness and energy loss due to various forms of fractures. That is why this technique has become essential to investigate and enhance to turn it into a valuable complementary tool for physicians to improve fracture severity understanding, follow healing, and make better-informed treatment choices without undue exposure to radiation.

The novelty in this work is that it systematically compares fracture orientation (lateral, longitudinal, oblique L→R and R→L) effect with reference bone (unfractured) under experimental conditions using FRF, coherence, and phase shift analysis that have not been addressed in previous studies.

MATERIAL AND METHODS

Bone specimens

Sample collection and ethical approval

This research examined goat metacarpal bones which were obtained from slaughterhouses in Rajkot, Gujarat, India. The soft tissues were excised from the bones using a formaldehyde solution and kept it in air-dried to provide consistent preparation and convenience of handling during experiment. Ethical approval: ECR/356/Indt/GJ2022.

Bone specimen and fracture modeling

Figure 1 show five bone specimens (B1 to B5), each bone characterized by a different fracture orientation and bone length, used to evaluate structural integrity through vibration analysis. Artificial fractures were introduced using careful saw cuts on the external surface of bone (B2 to B5). The detailed bone and fracture parameters used in the experimental study are summarized in Table 1.

Data processing for bone fracture characterization

The excitation was applied using an instrumented impact hammer, and the vibrational response was recorded through an accelerometer. Both signals were acquired using a multichannel DAQ system and processed in Sigview software by employing fast Fourier transform (FFT) methods to obtain frequency response functions (FRFs), coherence, and phase. This approach is strongly established for structural dynamics and has been used before in bone mechanics research to analyze fracture healing as well as dynamic properties [28,29].

Signal transformation and frequency-domain analysis

The governing equation of force damped vibration structure, such as bone, subjected to an external force can be represented by classical second order differential equation of motion.

$$m\ddot{x}(t) + c\dot{x}(t) + kx(t) = F(t) \qquad (1)$$

where: m, c, and k are mass (kg), damping (Ns/m) and stiffness (N/m) of the system, respectively, $x(t)$ is the displacement (m), $\dot{x}(t), \ddot{x}(t)$ first and second derivatives of displacement i.e. velocity and acceleration

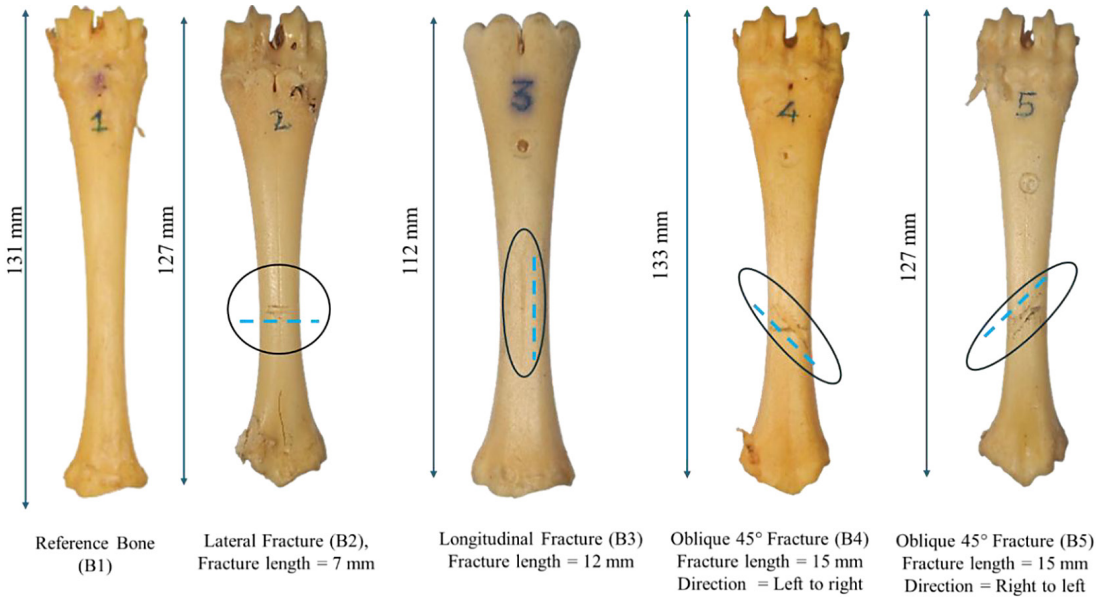

Figure 1. Fracture orientations on bone

Table 1. Parameters of bone specimen and fracture

Specimen ID	Fracture orientation	Fracture length (mm)	Bone length (mm)
B1	Reference bone	0	131
B2	Fracture perpendicular to bone axis	7	127
B3	Fracture parallel to bone axis	12	112
B4	45°Oblique fracture (Left to right)	15	133
B5	45°Oblique fracture (Right to left)	15	127

response and $F(t)$ is external force (N) applied using an impact hammer at free end of bone, t is time in second.

In the frequency domain analysis, commonly used in impact testing, this governing Equation 1 needs to be converted into frequency domain of equation in to force vibration transformed using Fourier transformation which results in

$$(-\omega^2 m + j\omega c + k)\, X(\omega) = F(\omega) \qquad (2)$$

Solving for transfer function for Frequency response function (FRF)

$$H(\omega) = \frac{X(\omega)}{F(\omega)} = \frac{1}{k-\omega^2 m+j\omega c} \qquad (3)$$

where: $H(\omega)$ is frequency response function (FRF), ω is angular frequency (rad/s), $\omega = 2\pi f$, j is imaginary unit, and $X(\omega)$ and $F(\omega)$. Fourier transformation of displacement and force respectively. When using accelerometer to measure acceleration, the input form of FRF is used

$$H_a(\omega) = \frac{A(\omega)}{F(\omega)} = \frac{\omega^2}{k-\omega^2 m+j\omega c} \qquad (4)$$

where: $H_a(\omega)$ is the acceleration over force FRF (g/N), $A(\omega)$ is Fourier transform of acceleration response (m/s²) in the frequency domain, directly measured by the sensor, $F(\omega)$ Fourier transform of impact force (N).

Such relationship enables the stiffness, damping, and resonant frequency behavior of bone structures to be measured under various conditions of fracture. Ewins [29] offered a detailed description of this theory applied to experimental modal analysis and impact testing. Kotowski et al. [30] also presented the practical measurement of FRFs by impulse response methods, especially applicable to experimental arrangements with impact hammers and accelerometers. Pérez et al. [31] expound on the mathematical modeling of FRF matrices and their application in dynamic system identification, while Rho et al. [32] use these concepts to analyze the mechanical behavior of a human bone, with

emphasis on how alterations in structural integrity influence dynamic response. These studies together provide the theoretical basis for the application of frequency response functions as a non-invasive tool in the analysis of bone fracture.

Experimental system layout and process for data collection

The experimental setup begins with the Impact Hammer (Figure 2a), which uses a controlled force impulse on the bone specimen. This hammer includes an in-built force sensor with a sensitivity of 2.25 mV/N, ensuring precise measurement of the impact force. The bone specimen (Figure 2b) was fitted with an accelerometer (Figure 2c) to capture vibration response. This sensor has a sensitivity of 100 mV/g and operates over a frequency range of 1 Hz to 10 kHz, which is suitable for high-resolution vibration measurements. The accelerometer sends real-time vibration signals through a signal conditioner (Figure 2d), which helps in amplifying the signals, filtering out noise, and stabilizing the readings. These signals passed through the Data Acquisition System (DAQ) (Figure 2e), which digitizes the input with 16-bit resolution, supports a high sampling rate of 500 kS/s, and can handle input ranges up to ±10V. Finally, the processed signals were sent to the computer installed with Sigview software (Figure 2f), where the data analyzed in real time. This integrated setup allows for efficient monitoring and interpretation of the bone's dynamic response under impact loading. In this experimental testing of bone specimens under different fracture orientation, a lightweight impact hammer (YMC-IH-01, 138 g) was employed. The hammer was released from a height of 15 cm, and using the relation $V = \sqrt{2gh}$, the average impact velocity was calculated as 1.17 m/s. This confirms that it corresponds to a low-velocity impact [33].

Experiment methodology

During dynamic testing of bone lateral impact applied on each bone. Each bone specimen (B1 to B5) was fixed using a mechanical clamp, with controlled lateral impact applied to the free end of the bone using an impact hammer, as illustrated in Figure 3. An accelerometer mounted near the fix end to measure the response. In each test, a controlled, accurate impact was used to achieve uniform force application. To compensate for variability and improve reliability, three trials of each fractured bone specimen performed, and the average result considered use in subsequent dynamic vibration analysis [8, 34]. The hammer input force and resultant output acceleration signals were recorded on a data acquisition system (DAQ) and observed in real time on Sigview software. The signals were further examined by calculating the frequency response function (FRF), coherence function, and phase shift behavior using the incorporated fast Fourier transform (FFT) tools in the software. This technique allowed precise measurement of dynamic behavior and

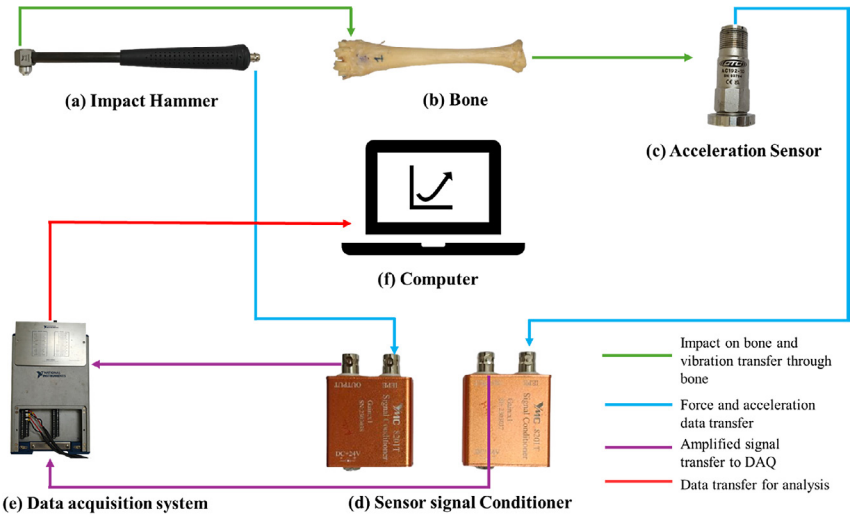

Figure 2. (a) Impact hammer (YMC-IH-01, DJB Instruments UK Ltd, UK), (b) bone specimen, (c) accelerometer (CTC-AC192-1D, CTC, USA), (d) sensor signal conditioner (CTC, USA), (e) data acquisition system (NI-USB 6341, National Instruments, USA), (f) computer equipped with Sigview software (Germany)

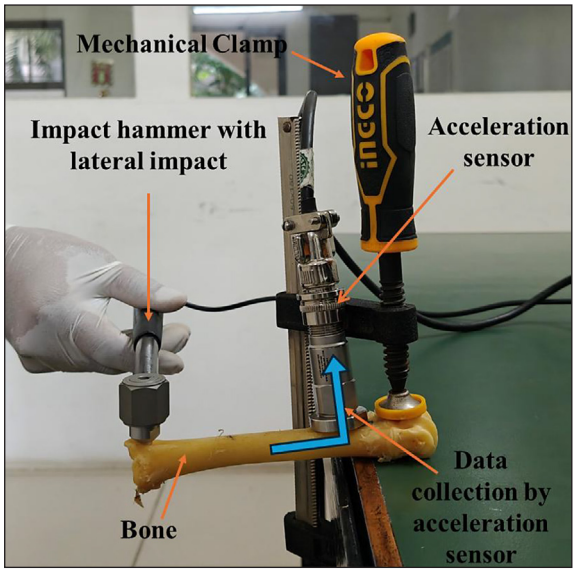

Figure 3. Experimental setup for lateral impact test on bone

reduced error due to variations in manual impact [35].

To maintain uniformity, the mechanical clamping setup was standardized across the specimens. The bone was mounted in mechanical vice, fixed with rubber cap (shown in orange color in Figure 3) and fate table to prevent slippage and damage. The jaw of the vice was tightened to a fixed position for all the tests, maintaining a constant clamping force. This process ensured that all the test specimens were subject to the same clamping force and reduced result variation. With the help of this arrangement reduced natural frequency variation in test results [36]. During actual in vivo experiments on human patients, bone would need to be fixed under a cantilever or simply supported condition when collecting vibration data. Such adaptations would improve the translations relevance of vibration-based diagnostic method for clinical applications [12,18,37].

RESULTS AND DISCUSSION

Reference bone: Case 1

The dynamic characterization of the reference bone (unfractured) evaluated through FRF, coherence, and phase shift analysis are shown in Figure 4. FRF as shown in Figure 4a of the reference bone specimen, and its dynamic behavior over three main control zones: stiffness, damping, and mass. Under the low-frequency range (0–50 Hz), the green-shaded response dominated by the stiffness of the bone. The reference bone has high stiffness and, therefore, a moderate to low FRF magnitude found in stiffness control zone. The curve with a peak magnitude of 4 g/N at 40 Hz, which was the first bending-type motion resonance. This zone establishes that the bone still has its elastic integrity. In the damping control range (50–80 Hz), filled in orange, the first major resonance peak at 62 Hz, with a magnitude of 27.26 g/N, which was the first natural frequency. Outside this range, in the mass control region (>80 Hz), the blue shaded area, the FRF response shows a steady fall, which means that system behavior is increasingly dominated by inertial effects. The curve becomes flat gradually, showing steady decay characteristic of mass-dominated behavior, without any evidence of aberrant mass-triggered vibrations evidence of mechanical stability in the bone. The coherence (Figure 4b) function is measure of the linearity and dependability of the input-output relationship. Over most of the frequency range above 100 Hz coherence value is near 1. This indicates linear and high-quality measurement from the reference bone. Small drops in coherence at 40 Hz and 62 Hz frequencies and tend to be due to phase wrapping or minor non-linearities. The phase response (Figure 4c) in degrees represent the phase difference between output acceleration and input force as a function of frequency. This sudden phase transition of about 62 Hz, which describes a change from to negative (-180°) to positive (+180°) phase change, typical identify resonance response. There are no phase discontinuities or irregular jumps beyond 62 Hz, which further supports the integrity and symmetry of the reference (unfractured) bone.

FRF, coherence, and phase analysis of the reference (unfractured) bone specimen establish mechanically stable and symmetric behavior. Noticeable stiffness, damping, and mass control zone (where the dynamic response is governed primarily by inertial properties) align with classical dynamic response theory [38]. The high coherence and phase consistency confirm experimental reliability. A resonance peak at 62 Hz indicates minimal damping and supports the structural integrity of the bone. These baseline characteristics provide a robust reference for comparative analysis with fractured specimens.

The influence of sensor mass on frequency response measurements is a critical factor when testing lightweight biological specimens, such as

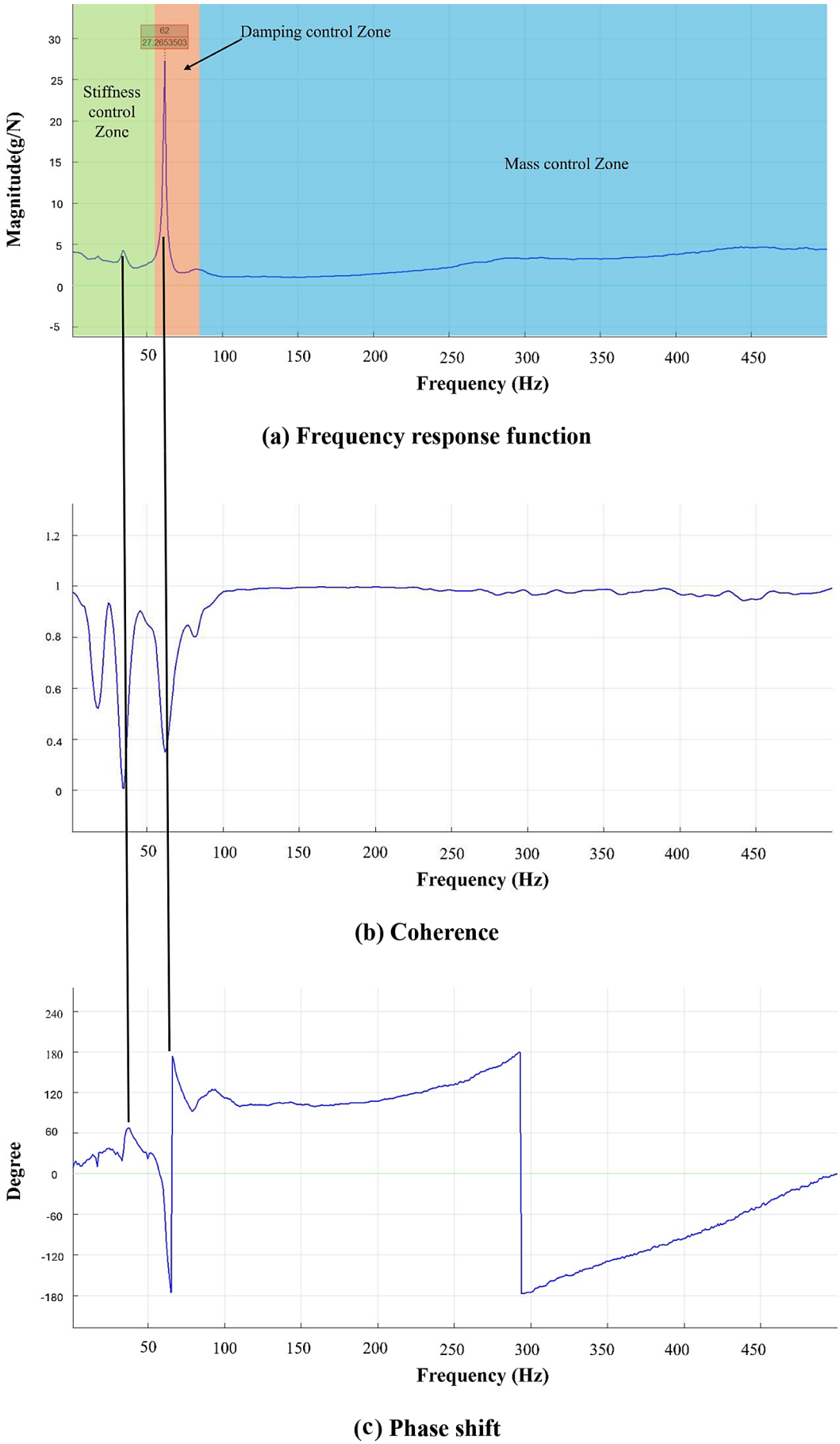

Figure 4. Frequency domain characterization of reference bone (B1) due to lateral impact

bones. In the conducted study, the CTC AC192-1D accelerometer was mounted near the fixed end of the specimen to minimize its effect, since this location undergoes lower modal displacement compared to the free end. Nevertheless, the relative weight of the accelerometer to the bone mass may still introduce a downward shift in measured natural frequencies. The literature has reported the same challenges. Yadav and Singh [39] showed that adding accelerometer-like masses at different locations on lightweight cantilever beams significantly altered their natural frequencies. Drvárová [40] further emphasized that when the sensor-to-structure mass ratio exceeds a certain threshold, measurement errors in modal frequencies become nontrivial. More recently, Scanlan et al. [41] demonstrated through vibro-acoustic excitation of bone specimens that careful selection of accelerometer weight is essential to ensure reliable modal analysis. Sensor placement is also an important consideration; studies indicate that mass loading at antinodes produces more pronounced shifts than at nodal positions [42]. To resolve these limitations, miniature MEMS-based accelerometers have been explored for vibration and bone-quality assessment, where their low mass and high sensitivity reduce bias in frequency response measurements while maintaining the accuracy of the signal measurement [43].

Under in vivo conditions, this method can be tested on human bone which is surrounded by soft tissues and joint constraints, that introduced damping and noise (due to muscles and skin) into vibration response. To address this noise, advanced signal process software which can help eliminate biological noise and extract bone-specific vibration feature is required [8, 12, 37].

Lateral fracture bone: Case 2

The dynamic characterization of the lateral fractured bone was evaluated through FRF, coherence, and phase shift analysis shown in Figure 5. Frequency response function (Figure 5a) plot assessed in three main regions: stiffness control, damping control, and mass control zone. The stiffness control zone (0 to 10 Hz) found in the low-frequency region of the FRF plot, with an initial magnitude of approximately 8 g/N higher than the corresponding magnitude 4 g/N observed in the reference bone. This response evaluated reduction in bending stiffness, which identified a direct lateral fracture impairing bone structure rigidity. The coherence (Figure 5b) in this zone drops actually below 1, suggesting nonlinearities likely induced by fracture face and reduced bone uniformity. The phase plot revealed early-phase disturbances and minor oscillations prior to the resonance transition, further supporting the presence of local stiffness degradation. In the damping control zone (11 to 30 Hz) resonance peak at 14 g/N magnitude and 30.35 Hz. Compared to the resonance peak magnitude 27.26 g/N of the reference bone, the lateral fractured bone found higher magnitude of 30.35 g/N and narrow bandwidth indicating increment in damping. This behavior found that energy dissipation mechanisms, such as frictional sliding at the fracture interface and microstructural discontinuities introduced by the fracture [44, 45]. The coherence in this region shows lowest values (~0), confirming poor linear correlation between excitation due to impact hammer and response due to acceleration sensor. The reason behind that involves localized energy losses and internal friction due to fractured surface on bone. The phase plot shows a clear and steep phase drop at the resonance frequency, which validates the existence of a primary natural frequency influenced by damping and stiffness loss. Mass control zone beyond resonance frequency in the range of above 31 Hz remain in wider bandwidth. FRF response transitioned into the mass-dominated regime, displaying a broad secondary peak near 350–375 Hz, followed by a gradual decay. This behavior reflects inertial coupling effects and potential mass redistribution due to the fracture, which alters the modal characteristics of the system [46]. In this region, the coherence stabilized and remained consistently above 0.90, indicate reliable linear behavior and minimal noise interference. The phase shift curve (Figure 5c) exhibited smooth and gradual transitions with distinct modal phase jumps at higher frequencies (~180 Hz and ~450 Hz), consistent with the presence of well-defined higher-order vibration modes. The combined FRF, coherence, and phase analyses collectively reveal the dynamic impact of a lateral fracture on bone vibrational behavior. The increased FRF magnitude and narrow resonance in the stiffness and damping zones confirm stiffness loss and elevated damping. Simultaneously, coherence dips and phase irregularities near resonance provide strong evidence of energy dissipation and nonlinear effects caused by the fracture. In the higher-frequency mass-dominated zone, a secondary inertial peak and

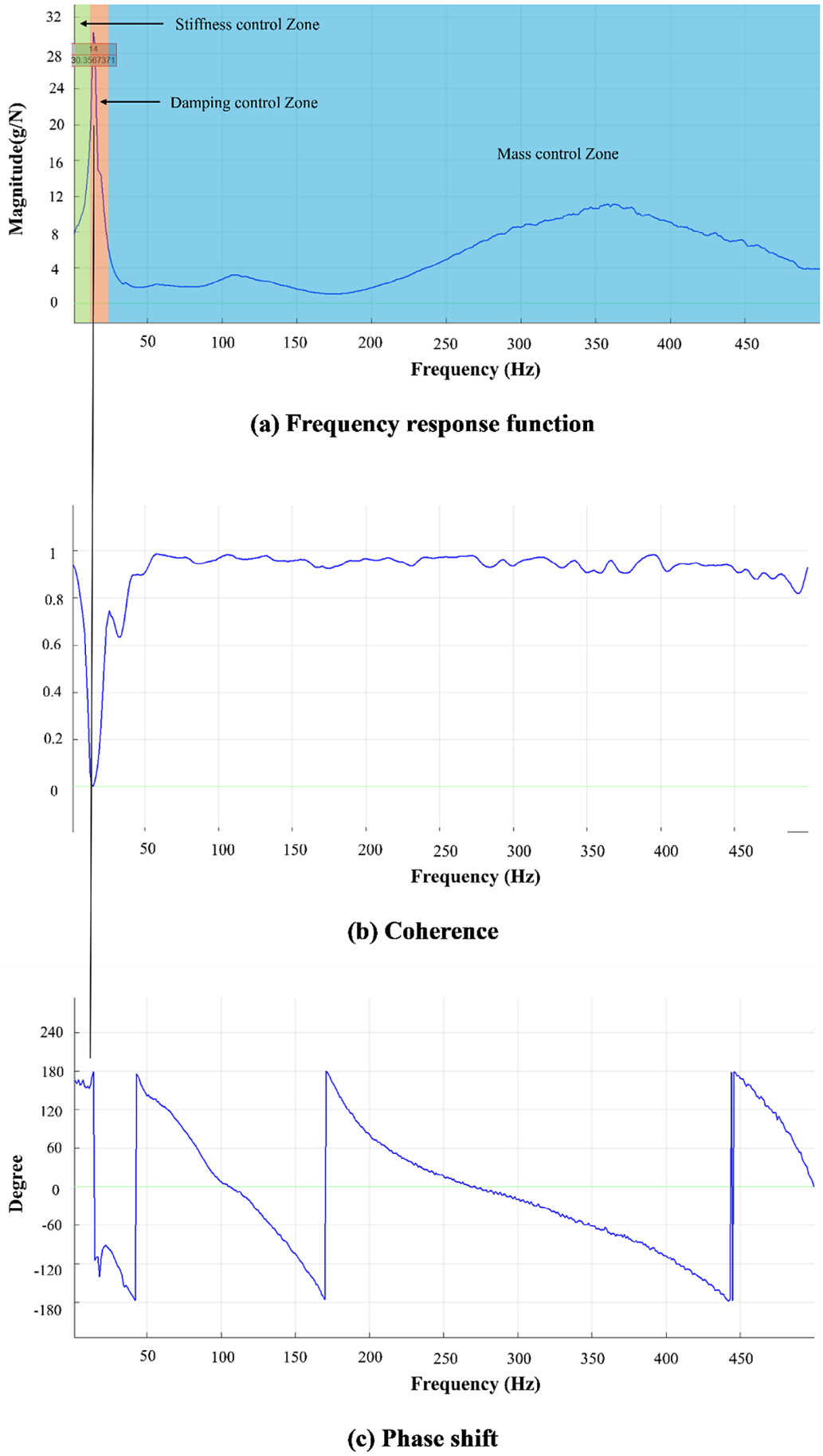

Figure 5. Frequency domain characterization of lateral fractured bone (B2) due to lateral impact

stable coherence indicate altered modal inertia but preserved overall system linearity.

Longitudinal fracture bone: Case 3

Figure 6 shows FRF, coherence and phase shift curve for longitudinal fractured bone. In the stiffness control zone, in which FRF (Figure 6a) ranging from 0 to 230 Hz, shaded green. The initial FRF magnitude 4 g/N at 130 Hz predominantly affect axial load paths, and under transverse bending, without causing severe stiffness loss. Coherence (Figure 6b) remains fairly high (>0.85) throughout this zone. The phase (Figure 6c) response remains generally stable with minor oscillations around the ±180° range, typical of a structure with low stiffness variations in this range. Damping Control Zone ranging from 230 to 270 Hz, shaded orange. A clear, narrow resonance peak is observed at 251 Hz with an amplitude of 10.3 g/N. The presence of a peak suggests low damping, as is typical in the structures where the fracture does not open and close cyclically under transverse loads [47]. Coherence dips briefly around the resonance frequency, which is 0.1, then recovers quickly to 0.95. A steep phase transition is observed precisely at the resonance frequency, which confirms the first mode shift and validates the natural frequency. The minor coherence drop near resonance is likely due to local interface movement and mild energy absorption. The bone structure still exhibits resonant behavior, with slight damping increase. The fracture introduces only localized dissipation effects. Mass Control Zone ranging greater than 270 Hz bandwidth, shaded blue. The magnitude decreases and steadily with no sharp irregularities, indicating mass-controlled inertial response. Minor undulations between 350 to 400 Hz indicate higher modes. The coherence dip in this frequency range is high, amounting to 0.82 and confirming mass distribution around fracture area and mode shape effect. The phase continues to descend smoothly, with modal transitions captured in 350 to 400 Hz. In this zone, the system behavior is governed by inertial properties, which are less affected by longitudinal cracks (as mass distribution remains symmetric). The mass control zone mostly unaffected, with smooth decay and stable inertial behavior. The dynamic response of the longitudinally fractured bone shows minimal disruption in the stiffness control zone, due to the crack orientation being parallel to the loading direction. The damping control zone displays a sharp resonance peak at 251 Hz, with only slight damping effects, reflected by a small coherence dip and clean phase shift. In the mass control zone, the system maintains smooth inertial response, validating structural symmetry of significant mass redistribution. Overall, the longitudinal fracture shows lesser severity in vibrational impact compared to lateral fractures, and this was well captured through FRF, coherence, and phase analysis.

Oblique fracture bone (45° Left to right): Case 4

The dynamic response of the obliquely fractured bone specimen was examined through FRF, coherence, and phase analyses in Figure 7. Frequency response function (Figure 7a) segmented across stiffness, damping, and mass control zones. In the stiffness control zone (0–250 Hz), the FRF magnitude remained relatively low, with a primary peak just under 4 g/N, and multiple minor resonances distributed across the range. This pattern identifies partial stiffness reduction due to the oblique fracture affecting both axial and flexural rigidity. The coherence plot (Figure 7b) shows a dip below 0.2 at 40 Hz, indicating nonlinear behavior and energy dispersion typical of bone structural discontinuities. Additionally, the phase response (Figure 7c) unveiled rapid oscillations and irregularity in this low-frequency range which support the presence of asymmetric compliance and disturbed stiffness

In the damping control zone ranging from 250 to 300 Hz there is a distinct resonance peak observed at 278 Hz with a magnitude of 9.96 g/N. This peak is relatively sharp, which was broader than seen in longitudinal fractures but narrow than in lateral fracture, suggesting moderate damping characteristics. A sharp drop in coherence value zero (0) at the resonance frequency coincided with a steep phase shift, confirming energy dissipation effects associated with the oblique fracture. The damping attributed to frictional sliding and intermittent fracture closure during dynamic excitation, which characterize the oblique fractures involving both shear and tensile components [48].

In the mass control zone (above 300 Hz), the FRF revealed multiple high-frequency peaks – particularly around 340 Hz, 425 Hz indicating excitation of higher-order vibration modes. Unlike the smoother decay seen in reference and lateral fractured bones. The oblique fracture identifies significant modal complexity. This analysis

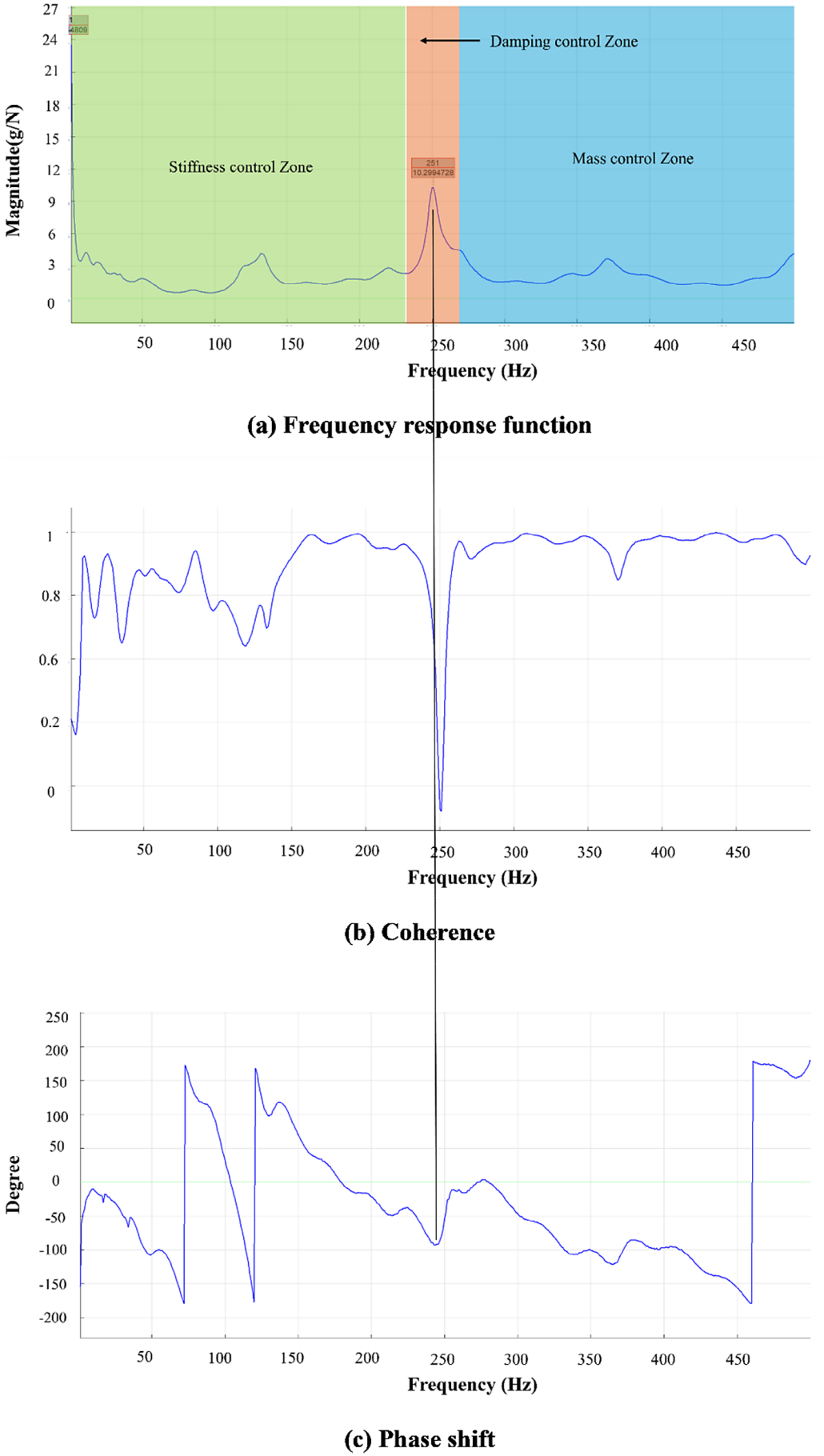

Figure 6. Frequency domain characterization of longitudinal fractured bone (B3) due to lateral impact

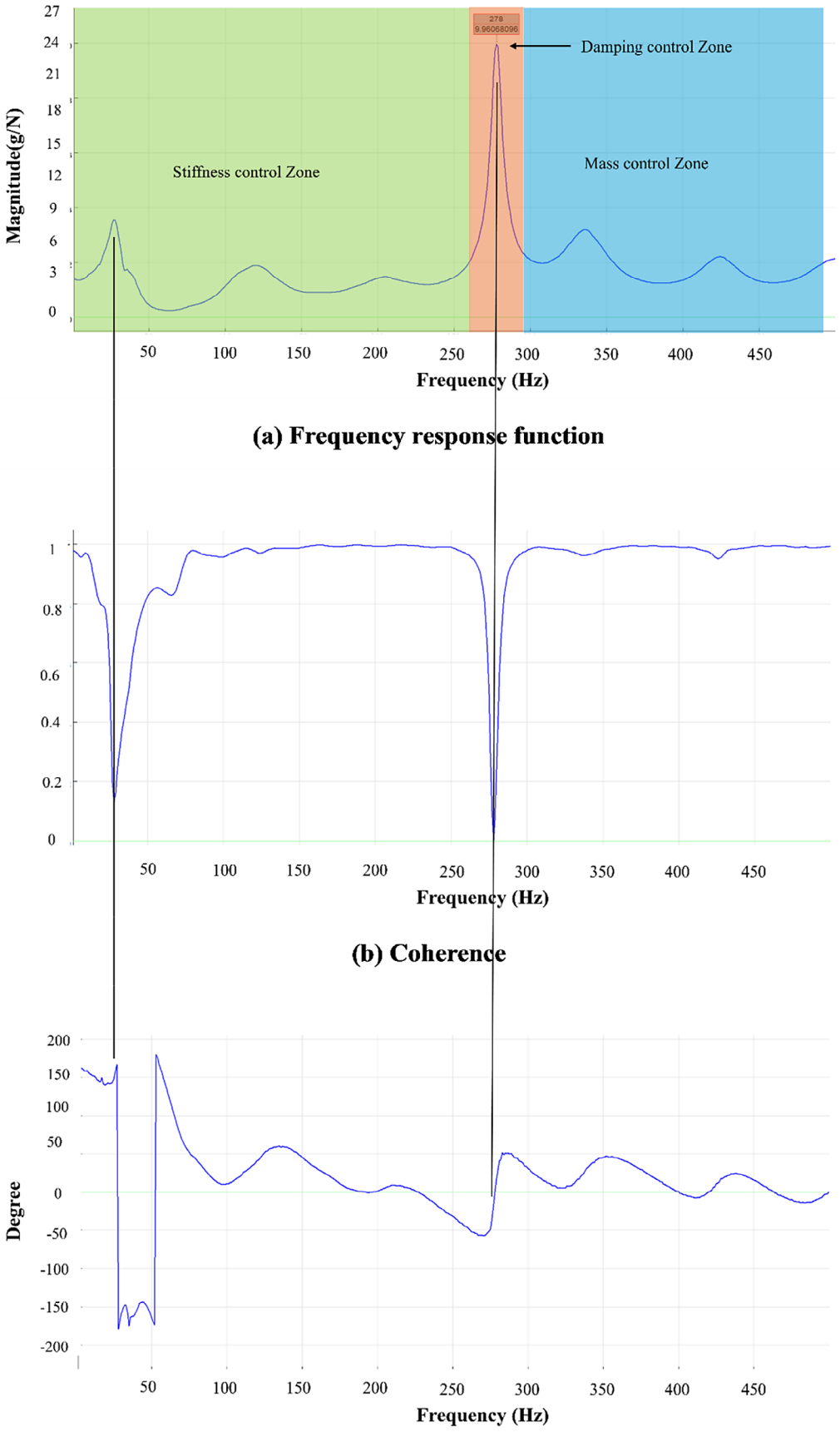

Figure 7. Frequency domain characterization of oblique fractured bone (45° left to right) (B4) due to lateral impact

is further supported by the stable near undulating coherence (>0.90) and rippled phase shifts in this region. These features suggest localized mass redistribution and inertial imbalance due to asymmetric fracture geometry. Overall, the oblique fracture validates a combined effect of moderate stiffness loss, intermediate damping, and distorted inertial response, capturing the hybrid vibrational behavior introduced by its oblique orientation.

Oblique fracture bone (45° right to left): Case 5

The vibrational behavior of the obliquely fractured bone (45° right to left) is evaluated by frequency response function (FRF), coherence, and phase analyses in Figure 8. In the frequency response function (Figure 8a) across the stiffness, damping, and mass control zones. In the stiffness control zone in range from 0–230 Hz, the FRF plot reveals a relatively low-to-moderate initial magnitude, with a small peak at 10 Hz and another modest resonance at 160 Hz, suggesting a partially degraded stiffness profile. These localized peaks imply that the oblique fracture influences both bending and axial rigidity, but does not result in complete stiffness loss. The coherence (Figure 8b) remains high (>0.95) across most of the stiffness zone, although it briefly dips near the resonant peaks zero (0) at 10 Hz and 0.35 at 160 Hz, and the phase (Figure 8c) exhibits gradual transitions and minor fluctuations. These results collectively indicate moderate stiffness degradation, with mixed directional compliance introduced by the angular path of the fracture.

In the damping control zone ranging from 230 to 270 Hz, FRF exhibits a sharp and dominant resonance peak at 234 Hz, with a magnitude of 50.89 g/N, a notably higher than in other fracture types. This suggests that the oblique fracture contribute less energy dissipation in this orientation, resulting in low effective damping. However, the coherence plot displays a clear drop near the resonance frequency, confirming a minor degree of nonlinear energy loss and transient fracture surface interaction. The phase plot demonstrates a sharp transition of nearly −180° to +180°, validating the modal shift and confirm the presence of a dominant natural frequency in this region.

Beyond 250 Hz, FRF enters the mass control zone, where the magnitude begins to flatten with mild undulations and consistent behavior. Although multiple higher-order modal responses are visible (notably around 400–450 Hz), the FRF curve remains relatively stable and does not exhibit abrupt peaks or decays. The coherence continues to remain above 0.9, with some mild dips aligned with those high-frequency (400–450 Hz) peaks, indicating reliable measurements despite modal complexity. The phase response in this zone shows clear modal phase jumps and slow slopes, typical of a system with symmetric mass distribution and medium modal interference. Overall, the oblique right-to-left fracture present low damping, moderate stiffness weakening, and stable inertial response, suggesting that the fracture orientation maintains partial structural continuity while still disrupting the vibrational energy path across the transverse section.

Figure 9 indicates FRF vs. magnitude, indicating the vibrational response characteristics of bone specimens with different fracture orientations by comparing their resonance frequencies (FRF in Hz) and response magnitudes (g/N). The reference bone (B1), which is unfractured, exhibits a moderate resonance frequency of 62 Hz and a corresponding magnitude of 27.26 g/N, indicating healthy bone. In contrast, the lateral fracture bone (B2) shows a considerable drop in frequency to 14 Hz and an elevated magnitude of 30.35 g/N with a narrow FRF graph. This suggests a significant loss of stiffness, and the sharp peak of the FRF graph indicating a severe loss of damping in the bone. This indicates the bone becomes less stable and may have a chance to break with high impact force. In the same lateral fracture, bone (B2) has higher structural compliance, marking it as the most severely damaged condition. The longitudinal fracture (B3) found a high natural frequency of 251 Hz but a much lower magnitude of 10.3 g/N, indicating relatively preserved stiffness but reduced energy transmission due to fracture alignment with the force path. The oblique fractured bone (B4) (left to right) identifies the highest resonance frequency of 278 Hz with a low magnitude of 9.96 g/N, suggesting good stiffness retention with moderate damping conditions, whereas the oblique fractured bone (B5) (right to left) has a frequency of 234 Hz but the highest magnitude among all the fractured conditions of 50.89 g/N, indicating intense vibrational energy transmission due to unstable fracture interaction and incomplete closure. Overall, the graph clearly indicates that fracture orientation plays a substantial role in dynamic stiffness, damping, and energy dissipation. Among all, the lateral fracture presents the most severe mechanical degradation,

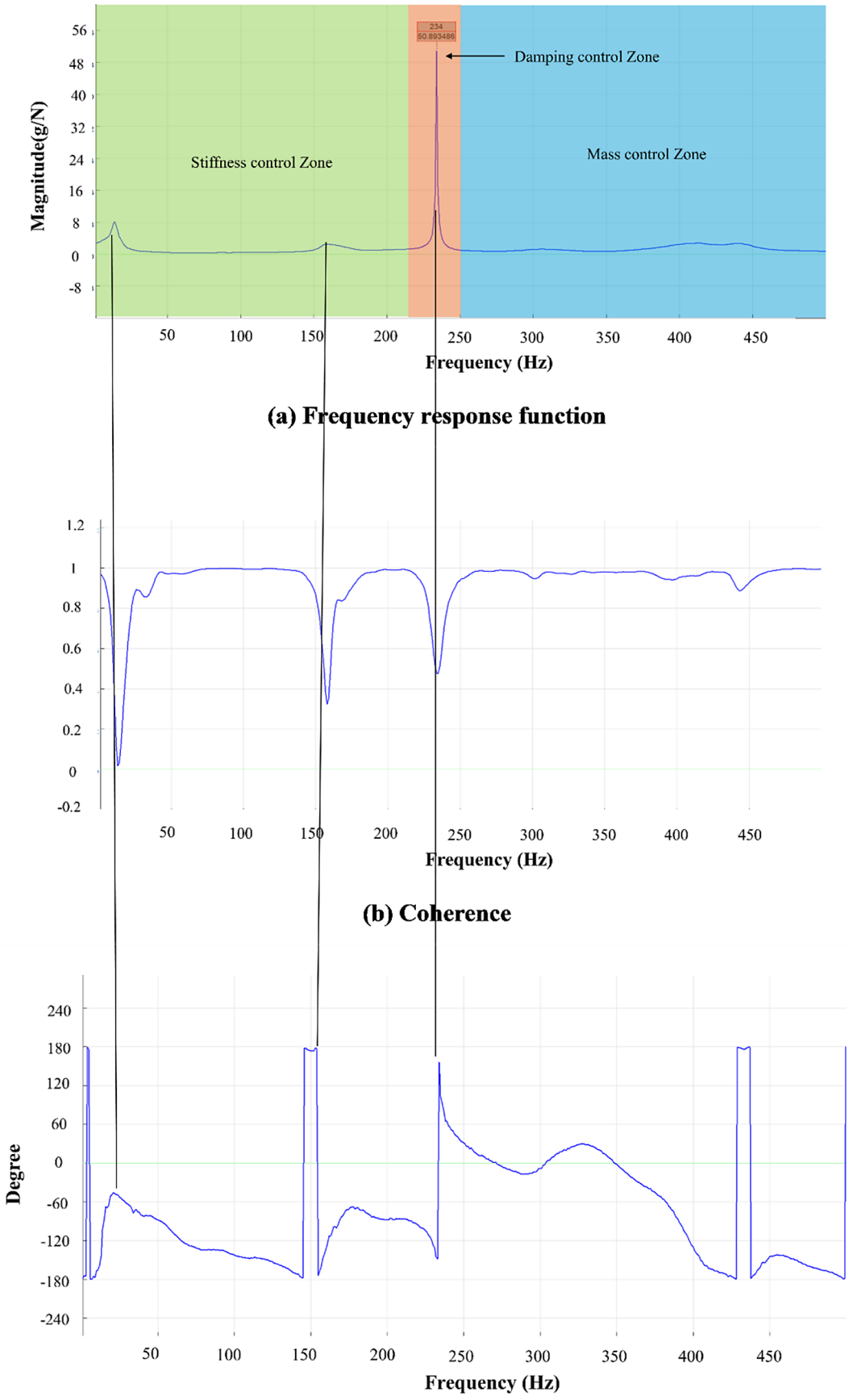

Figure 8. Frequency domain characterization of oblique fractured bone (45° right to left) (B5) due to lateral impact

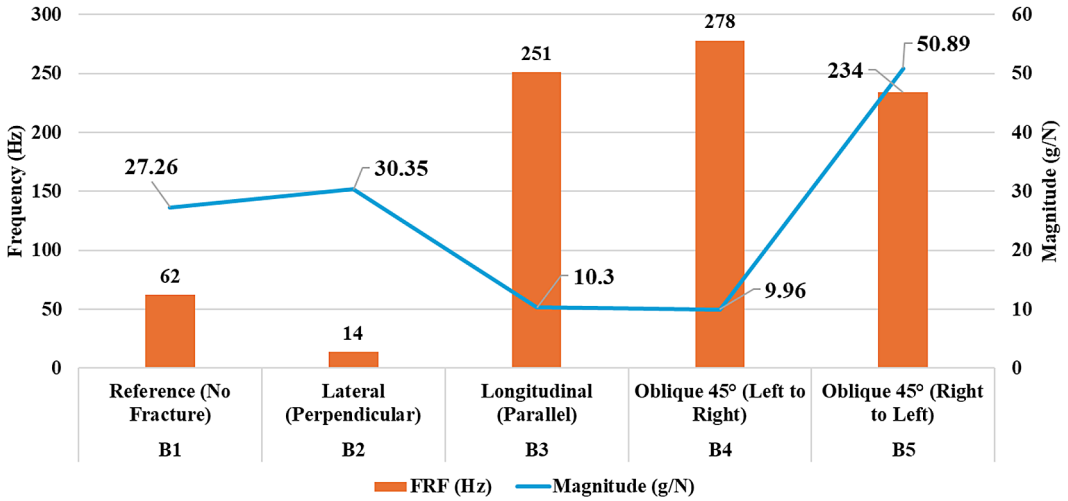

Figure 9. Frequency response function (FRF) resonance frequencies and peak magnitudes for bone specimens with various fracture orientations, illustrating changes in stiffness and damping due to fracture severity

while the oblique R→L fracture exhibits the highest vibrational sensitivity.

Having reference data of non-damaged bone remains one of the greatest challenges in clinical translation, since such values inevitably are patient-specific and vary with factors such as sex, age, bone density, and even diseases such as osteoporosis. Having standard databases derived by clinical and demographic variables is one potential solution, while employing an opposite (healthy) limb as a baseline is another [49]. Earlier studies have also demonstrated the viability of vibration-based techniques in this situation. Yoon et al. [12] considered transverse vibration responses for diagnosing fractures, Ali [37] illustrated bone vibration analysis as a fracture screening tool for long bones. Also, Sim et al. [8] showed experimentally that boundary conditions play an important role in the vibrational properties of fractured bones, showing the relevance of patient-specific reference data for correct diagnosis.

CONCLUSIONS

The findings show preliminary evidence that fracture orientation significantly influences bone vibrational behavior. Although this study was limited to five specimens with different boundary conditions (Lateral, longitudinal and 45° oblique fracture), the outcome indicated of these results founded vibration-based method as auxiliary technique for fracture assessment, Though, further validation is required through studies with extensive sample sizes, including classification by sex and body weight categories, to demonstrate large clinical relevancy. Using non-invasive lateral impact testing combined with FRF analysis, experiments evaluate how different fracture types affect stiffness, damping, and energy transmission. Among all specimens, the lateral fracture bone (B2) exhibited the most severe dynamic degradation, with a resonance frequency significantly reduced to 14 Hz compared with the reference (unfractured) bone (B1) at 62 Hz. Additionally, the lateral fracture showed the highest FRF peak magnitude of 30.35 g/N, indicating a major loss of structural stiffness and reduced damping ability, which is clearly shown in the FRF graph with a narrow spike in bandwidth (sharp resonance peak in the FRF indicates low damping and high dynamic sensitivity). In contrast, the longitudinal fracture (B3) resonance frequency shifted toward the high-frequency range at 251 Hz with a lower peak magnitude of 10.3 g/N, suggesting better stiffness preservation and minimal damping effects due to the fracture being aligned with the vibration signal transmission direction. The oblique fractures exhibited intermediate behavior: the left-to-right oblique fracture (B4) peaked at 278 Hz with a moderate FRF magnitude of 9.96 g/N, while the right-to-left oblique fracture (B5) showed a dominant resonance at 234 Hz and the highest magnitude among all fractured specimens at 50.89 g/N, indicating intense vibrational energy transmission and possible instability at the fracture interface. Overall, the present findings verify that lateral fractures place the greatest

compromise on bone integrity under damping conditions. This vibration-based method can effectively tell how serious a fracture is by using measurable factors, making it a useful, safe tool for checking bones that adds more information than regular imaging techniques.

Acknowledgements

The authors thankful to the funding support in this research by NewGen IEDC Centre (Government of India) and Marwadi University, Rajkot, for providing the academic platform and infrastructure facilities necessary to conduct the experiments.

REFERENCES

1. Khan SA, Khan MA, Song OY, Nazir M. Medical imaging fusion techniques: a survey benchmark analysis, open challenges and recommendations. Journal of Medical Imaging and Health Informatics. 2020 Nov 1;10(11):2523–31. https://doi.org/10.1166/jmihi.2020.3222
2. Wang G, Yu H, De Man B. An outlook on x-ray CT research and development. Medical physics. 2008 Mar;35(3):1051–64. https://doi.org/10.1118/1.2836950
3. Lipmann RK. The use of auscultatory percussion for the examination of fractures. J Bone Joint Surg 1932;14:118
4. Van der Perre G, Lowet G. In vivo assessment of bone mechanical properties by vibration and ultrasonic wave propagation analysis. Bone. 1996 Jan 1;18(1):S29–35. https://doi.org/10.1016/8756-3282(95)00377-0
5. Lowet G, Van der Perre G. Ultrasound velocity measurement in long bones: measurement method and simulation of ultrasound wave propagation. Journal of biomechanics. 1996 Oct 1;29(10):1255-62. https://doi.org/10.1016/0021-9290(96)00054-1
6. Bossy E, Talmant M, Laugier P. Effect of bone cortical thickness on velocity measurements using ultrasonic axial transmission: A 2D simulation study. The Journal of the Acoustical Society of America. 2002 Jul 1;112(1):297–307. https://doi.org/10.1121/1.1480836
7. Chen II, Saha S. Wave propagation characteristics in long bones to diagnose osteoporosis. Journal of biomechanics. 1987 Jan 1;20(5):523–7. https://doi.org/10.1016/0021-9290(87)90252-1
8. Sim SG, Woo YJ, Kim DY, Hwang SJ, Hwang KT, Lee CH, Yoon GH. Experimental study of the effect of the boundary conditions of fractured bone. Journal of the Mechanical Behavior of Biomedical Materials. 2021 Dec 1;124:104801. https://doi.org/10.1016/j.jmbbm.2021.104801
9. Safaei M, Bolus NB, Erturk A, Inan OT. Vibration characterization of the human knee joint in audible frequencies. Sensors. 2020 Jul 25;20(15):4138. https://doi.org/10.3390/s20154138
10. Do HD, Hong D, Park KS. Advanced assessment of the bone mineral density of a finger using a vibration-based in vivo device and two-stepped cantilever beam model. Journal of Mechanical Science and Technology. 2022 Jun;36(6):2811-6. https://doi.org/10.1007/s12206-022-0513-z
11. Razaghi H, Saatchi R, Offiah A, Bishop N, Burke D. Spectral analysis of bone low frequency vibration signals. In2012 8th International Symposium on Communication Systems, Networks & Digital Signal Processing (CSNDSP) 2012 Jul 18, 1-5. IEEE. https://doi.org/10.1109/CSNDSP.2012.6292718
12. Yoon GH, Woo YJ, Sim SG, Kim DY, Hwang SJ. Investigation of bone fracture diagnosis system using transverse vibration response. Proceedings of the Institution of Mechanical Engineers, Part H: Journal of Engineering in Medicine. 2021 May;235(5):597–611. https://doi.org/10.1177/0954411921997575
13. Chittibabu V, Rao SK, Rao GP. Factors affecting the mechanical properties of compact bone and miniature specimen test techniques: a review. Advances in Science and Technology. Research Journal. 2016;10(32). https://doi.org/10.12913/22998624/65117
14. Pattijn V, Van Lierde C, Van der Perre G, Naert I, Vander Sloten J. The resonance frequencies and mode shapes of dental implants: Rigid body behaviour versus bending behaviour. A numerical approach. Journal of biomechanics. 2006 Jan 1;39(5):939–47. https://doi.org/10.1016/j.jbiomech.2005.01.035
15. Nokes LD. The use of low-frequency vibration measurement in orthopaedics. Proceedings of the Institution of Mechanical Engineers, Part H: Journal of Engineering in Medicine. 1999 Mar 1;213(3):271–90. https://doi.org/10.1243/0954411991534979
16. Scanlan J, Umnova O, Li F. FE Modelling tibia bone vibration–the influence of shape, twist, and size. In Proceedings of the 10th Convention of the European Acoustics Association Forum Acusticum 2023,1305–1311. https://www.doi.org/10.61782/fa.2023.1141
17. Guo Z, Guo Z, Liang X, Liu S. A novel testing system for biomechanical evaluation of the bone or bone fixator. Sensor Review. 2018 Jul 3;38(4):405-11. https://doi.org/10.1108/SR-11-2017-0234
18. Mattei L, Di Puccio F, Marchetti S. Fracture healing monitoring by impact tests: single case study of a fractured tibia with external fixator. IEEE journal of translational engineering in health and medicine. 2019 Mar 15;7:1–6. https://doi.org/10.1109/JTEHM.2019.2901455

19. Verdenelli L, Rossetti R, Chiariotti P, Martarelli M, Scalise L. Experimental and numerical dynamic characterization of a human tibia. InJournal of Physics: Conference Series 2018 Dec 1;1149(1): 012029. IOP Publishing. 10.1088/1742-6596/1149/1/012029
20. Marco M, Belda R, Miguélez MH, Giner E. A heterogeneous orientation criterion for crack modelling in cortical bone using a phantom-node approach. Finite Elements in Analysis and Design. 2018 Jul 1;146:107–17. https://doi.org/10.1016/j.finel.2018.04.009
21. Behiri JC, Bonfield W. Orientation dependence of the fracture mechanics of cortical bone. Journal of biomechanics. 1989 Jan 1;22(8–9):863–72. https://doi.org/10.1016/0021-9290(89)90070-5
22. Dong XN, Acuna RL, Luo Q, Wang X. Orientation dependence of progressive post-yield behavior of human cortical bone in compression. Journal of biomechanics. 2012 Nov 15;45(16):2829–34. https://doi.org/10.1016/j.jbiomech.2012.08.034
23. Bone fractures. Cleveland Clinic. 2025. Available from: https://my.clevelandclinic.org/health/diseases/15241-bone-fractures
24. Ritchie RO, Kinney JH, Kruzic JJ, Nalla RK. A fracture mechanics and mechanistic approach to the failure of cortical bone. Fatigue & Fracture of Engineering Materials & Structures. 2005 Apr;28(4):345–71. https://doi.org/10.1111/j.1460-2695.2005.00878.x
25. Zimmermann EA, Busse B, Ritchie RO. The fracture mechanics of human bone: influence of disease and treatment. BoneKEy reports. 2015 Sep 2;4:743. https://doi.org/10.1038/bonekey.2015.112
26. Cohen H, Kugel C, May H, Medlej B, Stein D, Slon V, Brosh T, Hershkovitz I. The influence of impact direction and axial loading on the bone fracture pattern. Forensic science international. 2017 Aug 1;277:197–206. https://doi.org/10.1016/j.forsciint.2017.05.015
27. Gautam D, Rao VK. Nondestructive evaluation of mechanical properties of femur bone. Journal of Nondestructive Evaluation. 2021 Mar;40(1):22. https://doi.org/10.1007/s10921-021-00754-0
28. Kadhim AJ, Aubad MJ, Al-Juboori AM. Analyzing frequency response analysis experimentally for bone healing detection: examining the potential of vibrational evaluations. Diagnostyka. 2024;25. https://doi.org/10.29354/diag/192180
29. Ewins DJ. Modal testing: theory, practice and application. John Wiley & Sons; 2009 Jul 20.
30. Kotowski A. The method of frequency determination of impulse response components based on cross-correlation vs. fast Fourier transform. Diagnostyka. 2016;17(1):59–64.
31. Pérez MA, Serra-López R. A frequency domain-based correlation approach for structural assessment and damage identification. Mechanical Systems and Signal Processing. 2019 Mar 15;119:432–56. https://doi.org/10.1016/j.ymssp.2018.09.042
32. Rho JY, Hobatho MC, Ashman RB. Relations of mechanical properties to density and CT numbers in human bone. Medical engineering & physics. 1995 Jul 1;17(5):347–55. https://doi.org/10.1016/1350-4533(95)97314-F
33. Cohen H, Kugel C, May H, Medlej B, Stein D, Slon V, Hershkovitz I, Brosh T. The impact velocity and bone fracture pattern: forensic perspective. Forensic science international. 2016 Sep 1;266:54–62. https://doi.org/10.1016/j.forsciint.2016.04.035
34. Dewesoft. Dewesoft Modal Test & Analysis Manual. Trbovlje (Slovenia): Dewesoft; 2021. Available from: https://downloads.dewesoft.com/manuals/dewesoft-modal-test-analysis-manual-en.pdf
35. Siemens Digital Industries Software. What is a Frequency Response Function (FRF)? Plano (TX): Siemens; 2023. Available from: https://community.sw.siemens.com/s/article/what-is-a-frequency-response-function-frf
36. Skic A, Kołodziej P, Stropek Z, Beer-Lech K, Drabik K, Skic K et al. Analysis of the mechanical properties of femurs and eggshells of two selected Japanese quail lines under quasi-static and impact loading conditions. Advances in Science and Technology Research Journal. 2024;18(7):437–46. https://doi.org/10.12913/22998624/193625
37. Ali R. Bone vibration analysis as a novel screening tool for long bone fractures. Sheffield Hallam University (United Kingdom); 2019
38. Force response of a 1-DOF oscillator: regions of resonance. Available from: https://www.acs.psu.edu/drussell/Demos/Resonance-Regions/Resonance.html
39. Yadav A, Singh NK. Effects of accelerometer mass on natural frequency of a magnesium alloy cantilever beam. Vibroengineering Procedia. 2019 Nov 28;29:207–12. https://doi.org/10.21595/vp.2019.21114
40. Drvárová B, Dekýš V, Pijáková K. Effect of accelerometer mass on the natural frequencies of the measured structure. Transportation Research Procedia. 2023 Jan 1;74:740–7. https://doi.org/10.1016/j.trpro.2023.11.205
41. Scanlan J, Umnova O, Li F. Finite element modelling tibia bone vibration–the influence of shape, twist, and end scale. Acta Acustica. 2024;8:71. https://doi.org/10.1051/aacus/2024056
42. Takeshita A, Madrid J, Granillo E, Abdelkefi A. Insights on the impacts of accelerometer location on the dynamics and characteristics of complex structures. Sensors. 2023 Dec 14;23(24):9830. https://doi.org/10.3390/s23249830
43. Wang S, Wei X, Zhao Y, Jiang Z, Shen Y. A MEMS resonant accelerometer for low-frequency vibration

detection. Sensors and Actuators A: Physical. 2018 Nov 1;283:151–8. https://doi.org/10.1016/j.sna.2018.09.055

44. Dodge T, Wanis M, Ayoub R, Zhao L, Watts NB, Bhattacharya A, Akkus O, Robling A, Yokota H. Mechanical loading, damping, and load-driven bone formation in mouse tibiae. Bone. 2012 Oct 1;51(4):810–8. https://doi.org/10.1016/j.bone.2012.07.021
45. VanSchoiack LR, Wu JC, Sheets CG, Earthman JC. Effect of bone density on the damping behavior of dental implants: an in vitro method. Materials Science and Engineering: C. 2006 Sep 1;26(8):1307–11. https://doi.org/10.1016/j.msec.2005.08.019
46. Sinou J j., Lees AW. The influence of cracks in rotating shafts. Journal of Sound and Vibration. 2004 Dec 12;285(4–5):1015–37. https://doi.org/10.1016/j.jsv.2004.09.008
47. Bovsunovsky AP, Surace C. Considerations regarding superharmonic vibrations of a cracked beam and the variation in damping caused by the presence of the crack. Journal of Sound and Vibration. 2005 Dec 20;288(4–5):865–86. https://doi.org/10.1016/j.jsv.2005.01.038
48. Krack M, Bergman LA, Vakakis AF. On the efficacy of friction damping in the presence of nonlinear modal interactions. Journal of Sound and Vibration. 2016 May 26;370:209–20. https://doi.org/10.1016/j.jsv.2016.01.039
49. Skic A, Kołodziej P, Puzio I, Tymicki G, Beer-Lech K, Gołacki K. Methodological aspects of rat bone mechanical impact. Advances in Science and Technology Research Journal. 2022;16(6):140–6. https://doi.org/10.12913/22998624/156013